ACS OMEGA

Open Access

http://pubs.acs.org/journal/acsodf

Article

A Bifunctional Three-Dimensional Zn(II) Metal−Organic Framework with Strong Luminescence and Adsorption Cr(VI) Properties

Yufeng Chen, Shixiong Li,* Yubing Liu, Ping Shi, Shihua Xu,* and Yuejing Bin*

Cite This: *ACS Omega* 2024, 9, 18429−18437

Read Online

ACCESS | Metrics & More | Article Recommendations | Supporting Information

ABSTRACT: The mixed ligand 3-amino-1,2,4-triazole (Hatz) and terephthalic acid (H_2pta) reacted with $Zn(NO_3)_2{\cdot}6H_2O$ to synthesize a three-dimensional binuclear Zn(II) metal−organic framework: $\{[Zn_2{\cdot}(atz)_2{\cdot}(pta)]{\cdot}3H_2O\}_n$ (**3D-Zn-MOF**). This **3D-Zn-MOF** has two different types of pores (4.5 × 4.5 Å^2, 5.7 × 5.7 Å^2). The crystalline **3D-Zn-MOF** could be prepared into nanomaterials (**3D-N-Zn-MOF**) with particles of approximately 100 nm by a cell fragmentation apparatus. Compared with the solid-state luminescence of Hatz and H_2pta, it was found that **3D-N-Zn-MOF** exhibited strong luminescence performance and significant red-shift phenomenon. Due to the decrease in electronegativity and rigidity of ligands, as well as the effect of ligand metal charge transfer (LMCT), the fluorescence lifetime and quantum yield of **3D-ZN-N-MOF** were 2.7241 ns and 3.02%, respectively. The maximum experimental adsorption capacity of **3D-N-Zn-MOF** could reach 125.52 mg/g, which was superior to the majority of MOF adsorbents under the optimal adsorption conditions (25 °C, pH = 7, and the adsorbent concentration is 0.2000 g/L). The thermodynamic analysis of adsorption showed that the adsorption of Cr(VI) by **3D-N-Zn-MOF** was a spontaneous ($\triangle G < 0$) and exothermic ($\triangle H < 0$) process. It could be found that **3D-N-Zn-MOF** was a bifunctional material with potential applications by comprehensive analysis of the fluorescence and adsorption Cr(VI) performance.

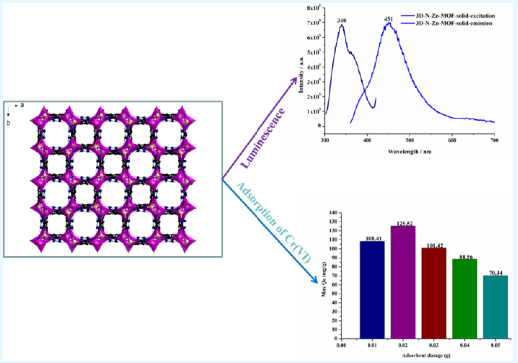

1. INTRODUCTION

Multifunctional materials can integrate multiple properties and functions, thereby demonstrating excellent performance in various aspects.[1−3] Developing multifunctional materials can provide more efficient and flexible solutions to energy and complex problems[1] and promote innovation and development in science and technology. This is of great significance for promoting sustainable development, improving the quality of life, and addressing major challenges.

Metal−organic frameworks (MOFs) are crystal structured materials composed of metal ions or metal clusters and organic ligands through coordination chemical reactions.[4] The basic structure of MOFs consists of metal ions (usually transition metals such as copper, zinc, and nickel) as centers, connecting multiple organic ligands (usually electron-rich organic acid molecules) to form a three-dimensional network.[5−7] The organic ligands of MOFs can form spatial configurations of different shapes and sizes through coordination with metal ions, which are called pores.[8] The pore structure of MOFs can be designed and regulated according to specific requirements, enabling MOFs to have highly adjustable functions such as adsorption,[9,10] separation,[11,12] photocatalysis,[13−15] and energy storage.[16−18] In addition, MOFs have many characteristics and advantages,[8−18] including high adjustability, large pore volume and surface area, porous structure, low density, and high chemical stability. These characteristics make MOFs have broad application potential in fields such as fluorescence,[19] adsorption,[20] gas separation,[12] catalytic reactions,[13−15] energy storage,[16−18] and sensing.[21−23] For example, fluorescent MOFs can achieve different fluorescence characteristics (optoelectronic devices, biological imaging, sensors) by selecting appropriate metal ions (Zn^{2+}, Cd^{2+}, Ag^{+}, and rare earth metal ions) and designing organic ligands. So, significant progress has been made in the research and development of MOFs, which have attracted widespread attention in various fields. They are considered the next generation of functional materials, providing new possibilities for addressing major challenges in fields such as energy, environment, and chemistry. Therefore, developing multifunctional metal−organic frameworks enables us to obtain materials with better performance and functionality, which can meet the needs of different fields. The development of this material will have extensive applications and promote scientific and technological progress in fields such as energy, environment, and medicine.

In this paper, a three-dimensional binuclear Zn(II) metal organic framework: $\{[Zn_2{\cdot}(atz)_2{\cdot}(pta)]{\cdot}3H_2O\}_n$ (**3D-Zn-**

Received: January 13, 2024
Revised: March 28, 2024
Accepted: March 29, 2024
Published: April 10, 2024

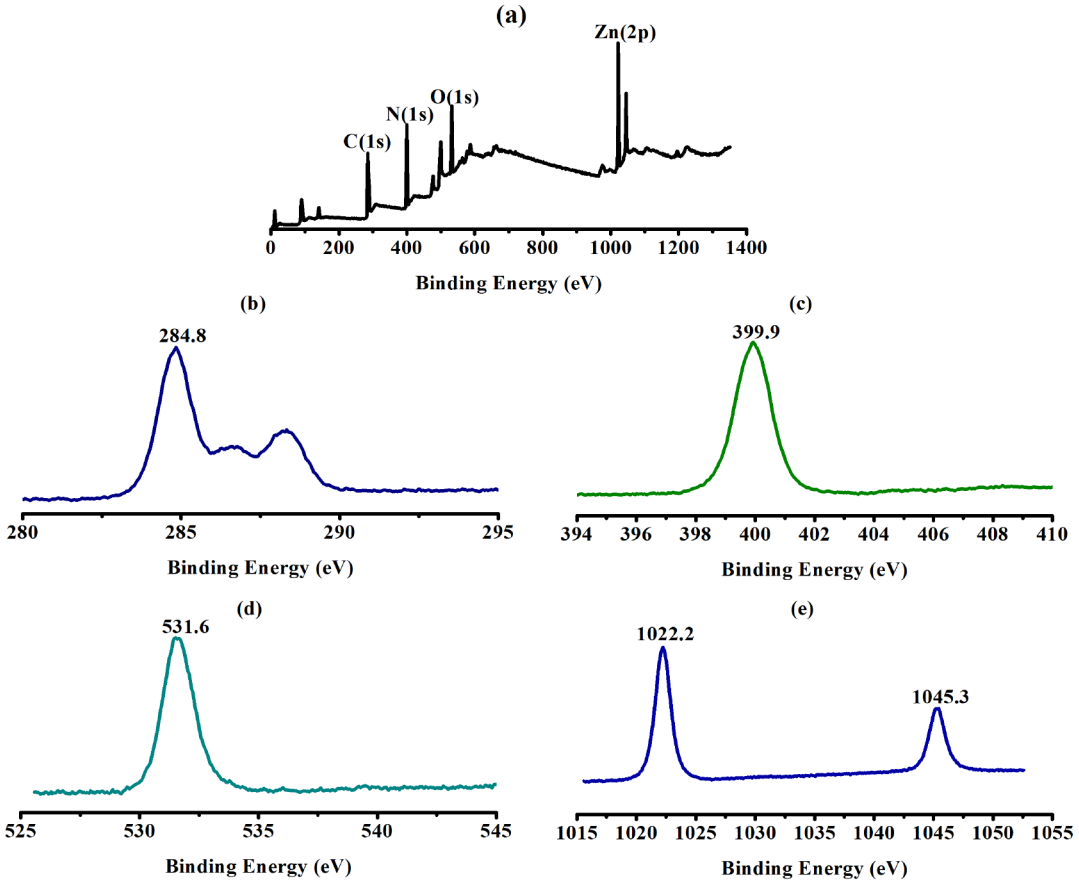

Figure 1. XPS of 3D-Zn-MOF: (a) Survey; (b) C(1s); (c) N(1s); (d) O(1s); (e) Zn(2p).

MOF), was synthesized by mixed ligands 3-amino-1,2,4-triazole (Hatz) and terephthalic acid (H_2pta) reacted with $Zn(NO_3)_2{\cdot}6H_2O$. The structure of **3D-Zn-MOF** was characterized by Fourier transform infrared (IR), elemental analysis, X-ray photoelectron spectroscopy (XPS), thermogravimetric analysis (TGA), and single crystal X-ray single crystal diffraction. The solid-state luminescence of the **3D-Zn-MOF** nanomaterial (**3D-N-Zn-MOF**) and the effects of adsorbent dosage, pH, and temperature on the adsorption performance of Cr(VI) were studied. The results showed that **3D-N-Zn-MOF** exhibited a strong performance of luminescence and adsorption of Cr(VI).

2. EXPERIMENTAL SECTION

2.1. Synthesis of $\{[Zn_2{\cdot}(atz)_2{\cdot}(pta)]{\cdot}3H_2O\}_n$ (3D-Zn-MOF). The Hatz (0.0841 g, 1.0 mmol), H_2pta (0.1661 g, 0.5 mmol), and $Zn(NO_3)_2{\cdot}6H_2O$ (0.2975 g, 1.0 mmol) were mixed in the solution of 8 mL *N,N*-dimethylformamide (DMF) and 2 mL water. The mixed solution was dispersed under ultrasound at room temperature. Then, it was transferred into a 23 mL polytetrafluoroethylene reactor liner. Finally, the mixed solution was heated in a 150 °C blast drying oven for 72 h. The mixed solution was naturally cooled to room temperature after the reaction heating was completed. Colorless block crystals of **3D-Zn-MOF** were obtained. Yield: 98.53%. (based on Zn^{2+}). Anal. Calcd for $C_6H_8O_{3.5}N_4Zn$: C, 27.96; H, 3.11; N, 21.74. Found: C, 28.01; H, 3.08; N, 21.77. IR (cm^{-1}) (Figure S1): 3416s, 3331m, 3233w, 2924w, 1665m, 1632w, 1586s, 1534w, 1397s, 1291m, 1284m, 1233s, 1154w, 1062s, 1016s, 892m, 839s, 747s, 749m, 576m, 498m.

2.2. X-Ray Diffraction. Diffraction data for **3D-Zn-MOF** were collected on a Bruker SMART CCD diffractometer (Mo Kα radiation, λ = 0.71073 Å) in Φ and ω scan modes. The anisotropic displacement parameters were applied to all non-hydrogen atoms in full-matrix least-squares refinements based on F2, which was performed by SHELXL-2013. The structure was solved by direct methods using Olex2 program.[24] The guest molecules were removed through SQUEEZE in structure refinement due to disorder. Anisotropic thermal parameters were assigned to all non-hydrogen atoms. The hydrogen atoms were placed at calculated positions and refined as riding atoms with isotropic displacement parameters. Crystallographic data and structure processing parameters for **3D-Zn-MOF** are summarized in Table S1. Selected bond lengths and bond angles for **3D-Zn-MOF** are listed in Table S2. The hydrogen bonds of **3D-Zn-MOF** are listed in Table S3, CCDC:2313254, **3D-Zn-MOF**.

2.3. Preparation of Nanoparticles (3D-N-Zn-MOF). 0.1000 g of **3D-Zn-MOF** (0.1000 g) was added to a 250 mL beaker. Next, added 100 mL of deionized water to the beaker. Shook the suspension solution in the beaker for 15 min by the cell crusher. Then, collected the solid powder precipitates by a high-speed centrifuge at 10 000 r/pm. Finally, the collected solid powder precipitates were placed in a 120 °C blast drying oven and heated for 12 h to obtain **3D-N-Zn-MOF**.

https://doi.org/10.1021/acsomega.4c00431
ACS Omega 2024, 9, 18429−18437

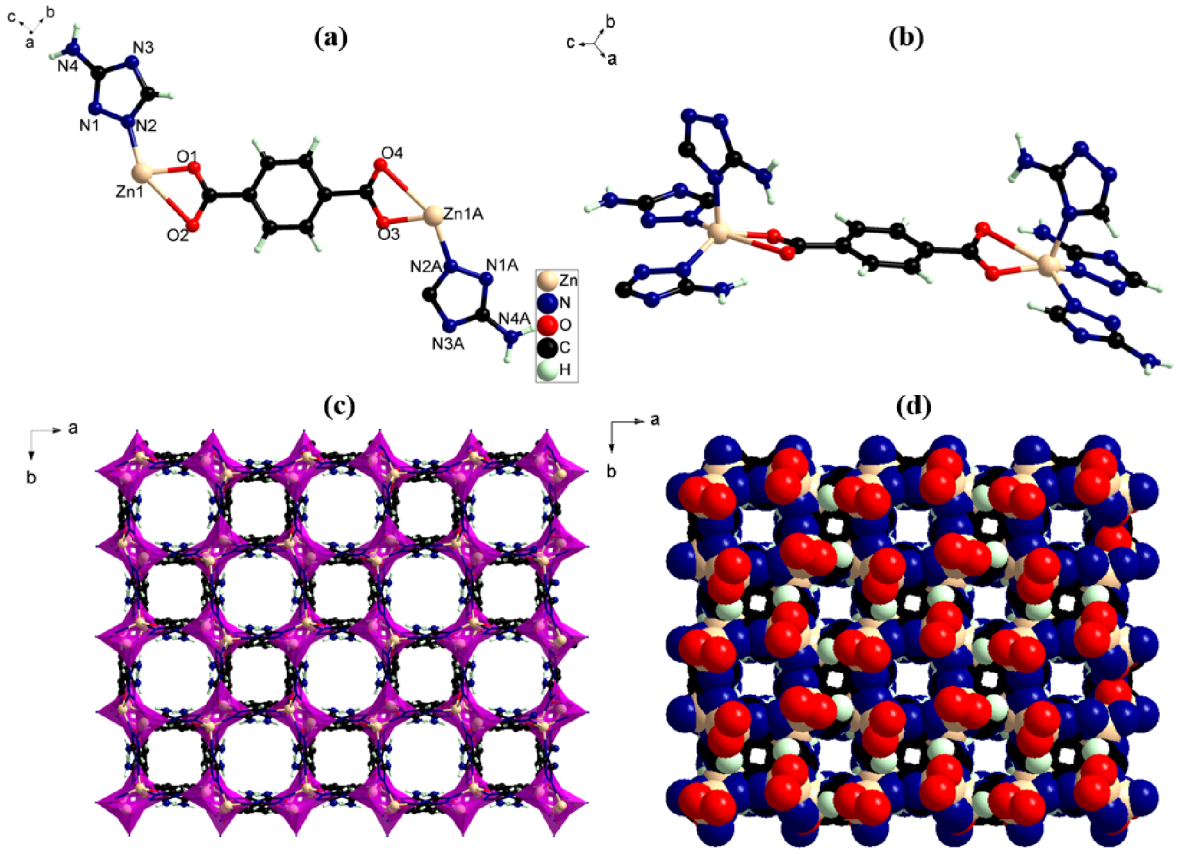

Figure 2. (a) Minimum independent structural unit of **3D-Zn-MOF**; (b) the coordination mode of Zn (II) in **3D-Zn-MOF**; (c) a 3D pore structure formed by ligand bridging; (d) 3D stacked structure.

3. RESULTS AND DISCUSSION

3.1. Structure of 3D-Zn-MOF. The elemental and valence state composition of **3D-Zn-MOF** was characterized and analyzed by X-ray photoelectron spectroscopy (XPS). The XPS of **3D-Zn-MOF** (Figure 1a) indicated that it was mainly composed of C, N, O, and Zn elements. The characteristic orbital peaks of C(1s), N(1s), and O(1s) were found at 284.8 eV (Figure 1b), 399.9 eV (Figure 1b), and 531.6 eV (Figure 1d), respectively. The characteristic orbital peak of Zn(2p) was observed at 1022.2 and 1045.3 eV (Figure 1e), which indicated that the zinc ions in **3D-Zn-MOF** were all Zn(II). The positions of these characteristic orbital peaks were all within the range reported in the literature.[19] However, XPS had not yet determined the structure of **3D-Zn-MOF**. Therefore, this requires the use of X-ray single crystal diffraction to determine its structure.

The structure of **3D-Zn-MOF** was analyzed by single-crystal X-ray single crystal diffraction. The results (Table S1) indicated that **3D-Zn-MOF** belonged to the tetragonal crystal system and *P*4/*nnc* space group, with a = 12.5961(5) Å, b = 12.5961(5) Å, c = 25.4618(12) Å, $\alpha = \beta = \gamma = 90.00°$, V = 4039.8(4) Å^3. The elemental and thermogravimetric analyses (Figure S2) showed the presence of solvent molecules in **3D-Zn-MOF**. The SQUEEZE analyses also revealed the presence of solvent molecules in crystal cells. A solvent mask was calculated, and 244 electrons were found in a volume of 1214 Å^3 in 2 voids per unit cell. This was consistent with the presence of 1.5[H_2O] per Formula Unit, which accounts for 240 electrons per unit cell. As a result,there was a single formula unit in the asymmetric unit, which was represented by the reported sum formula. In other words: Z was 16 and Z' was 1. The moiety formula was $C_6H_5N_4O_2Zn$,1.5[H_2O]. So, it was consisted of two Zn(II) ions, two atz$^-$ anions, and one pta^{2-} anion in the structure of **3D-Zn-MOF** after removing solvent molecules (Figure 2a). In **3D-Zn-MOF**, each Zn(II) ion (Figure 2b) coordinated with three N atoms (the N1^A, N2, N3^B were from different atz$^-$ anions), and two O atoms (the O1 and O2 were from pta^{2-} anion). Therefore, the coordination between Zn(II) and coordinating atoms in **3D-Zn-MOF** formed a ZnN_3O_2 square cone geometry (Figure S3a). Among them, the bond length range of Zn−N was 1.970(9)−2.042(9) Å (Zn(1)−N(1) = 1.970(9) Å, Zn(1)−N(3)^A = 2.029(9) Å, Zn(1)−N(2)^B = 2.042(9) Å, Zn(2)−N(5) = 1.982(9) Å, Zn(2)−N(7)^C = 2.059(9) Å, Zn(2)−N(6)^D = 2.019(9) Å). The two Zn−O bond lengths were Zn(1)−O(1) = 1.916(9) Å and Zn(2)−O(3) = 1.930 (9) Å, respectively. These bond lengths and bond angles were within the range of bond lengths and bond angles reported in literature for Zn complexes.[25−28] It is worth noting that a two-dimensional Zn-atz layer was formed by the atz$^-$ took μ_3-η^1:η^1:η^1 to coordinated with three Zn(II) atoms (Figure S3b). The adjacent Zn-atz two-dimensional layers were connected by pta^{2-} to form a three-dimensional structure (Figure 2c) with two different pores types of apertures (4.5 × 4.5 Å^2, 5.7 × 5.7 Å^2). The porosity of **3D-Zn-MOF** was calculated to be 27.5% by Platon software. According to topology analysis, the structure of the entire 3D-Zn-MOF could be described as a (3,4)-three-dimensional skeleton by simplifying the Zn(II) element into a single node. It was interesting that there were a large number of carboxyl O atoms on the surface of the stacked

https://doi.org/10.1021/acsomega.4c00431
ACS Omega 2024, 9, 18429−18437

structure of **3D-Zn-MOF** (Figure 2d), and these O functional groups could effectively affect the adsorption sites and performance.

3.2. Preparation and Physicochemical Properties of 3D-N-Zn-MOF. The crystalline **3D-Zn-MOF** could been prepared into nanomaterials (**3D-N-Zn-MOF**) with particles of approximately 100 nm (Figure S4a−d) by a cell fragmentation apparatus. The specific surface area, pore volume, and pore size distribution of **3D-N-Zn-MOF** were analyzed by N_2 adsorption/desorption experiments. The results (Figure S5, Table 1) indicated that it was a typical *S*-type adsorption isotherm. The BET surface area, pore volume, and pore size of the **3D-N-Zn-MOF** were 192.22 m^2/g, 0.47 cm^3/g, and 9.97 nm, respectively.

Table 1. N_2 Adsorption/Desorption Isotherms of 3D-N-Zn-MOF

parameter	value	parameter	value
single point surface area	188.57 m^2/g	BET surface area	192.22 m^2/g
t-plot micropore area	120.70 m^2/g	t-plot external surface area	71.51 m^2/g
pore volume	0.47 cm^3/g	pore size	9.97 nm

3.3. Fluorescence Performance of 3D-N-Zn-MOF. *3.3.1. Solid State Luminescence of Ligands and 3D-N-Zn-MOF.* The luminescent properties of Hatz and H_2PTA were tested at room temperature. The results (Figure 3a,b) indicated that the fluorescence intensities of these two ligands were relatively weak. Hatz was excited at 340 nm in the ultraviolet region, and it had a strong emission spectrum at 400 nm (Figure 3a). When H_2PTA was excited in the ultraviolet region at 350 nm, its emission spectrum reached its maximum peak at 430 nm (Figure 3b).

The above single-crystal X-ray diffraction analysis proved that Zn(II) had undergone a coordination reaction with ligands Hatz and H_2PTA, and **3D-Zn-MOF** was generated. Thus, some lone pair electrons on atz^- and PTA^{2-} were transferred to Zn(II) with empty orbitals. The XPS also proved that the zinc ions in **3D-Zn-MOF** were all Zn(II). The arrangement of extranuclear electrons in Zn(II) was $3d^{10}$. And literature[29] had also proven that Zn(II) complexes with a $3d^{10}$ arrangement typically exhibited good fluorescence performance. The solid-state fluorescence performance of **3D-N-Zn-MOF** was tested at room temperature. The results (Figure 3c) indicated that it had a strong emission spectrum at 451 nm when excited at 340 nm. By comparing the fluorescence properties with Hatz and H_2PTA, it was found that **3D-N-Zn-MOF** exhibited strong fluorescence intensity. In addition, **3D-N-Zn-MOF** showed a significant red-shift phenomenon. This was due to the transfer of electrons from the ligand (atz^- and PTA^{2-}) to central coordination Zn(II) in **3D-Zn-MOF**. At room temperature (298 K), **3D-N-Zn-MOF** was excited at 340 nm to measure its fluorescence lifetime. The results (Figure 3d) indicated that the fluorescence lifetime of **3D-N-Zn-MOF** was 2.7241 ns. This fluorescence lifetime was longer than most

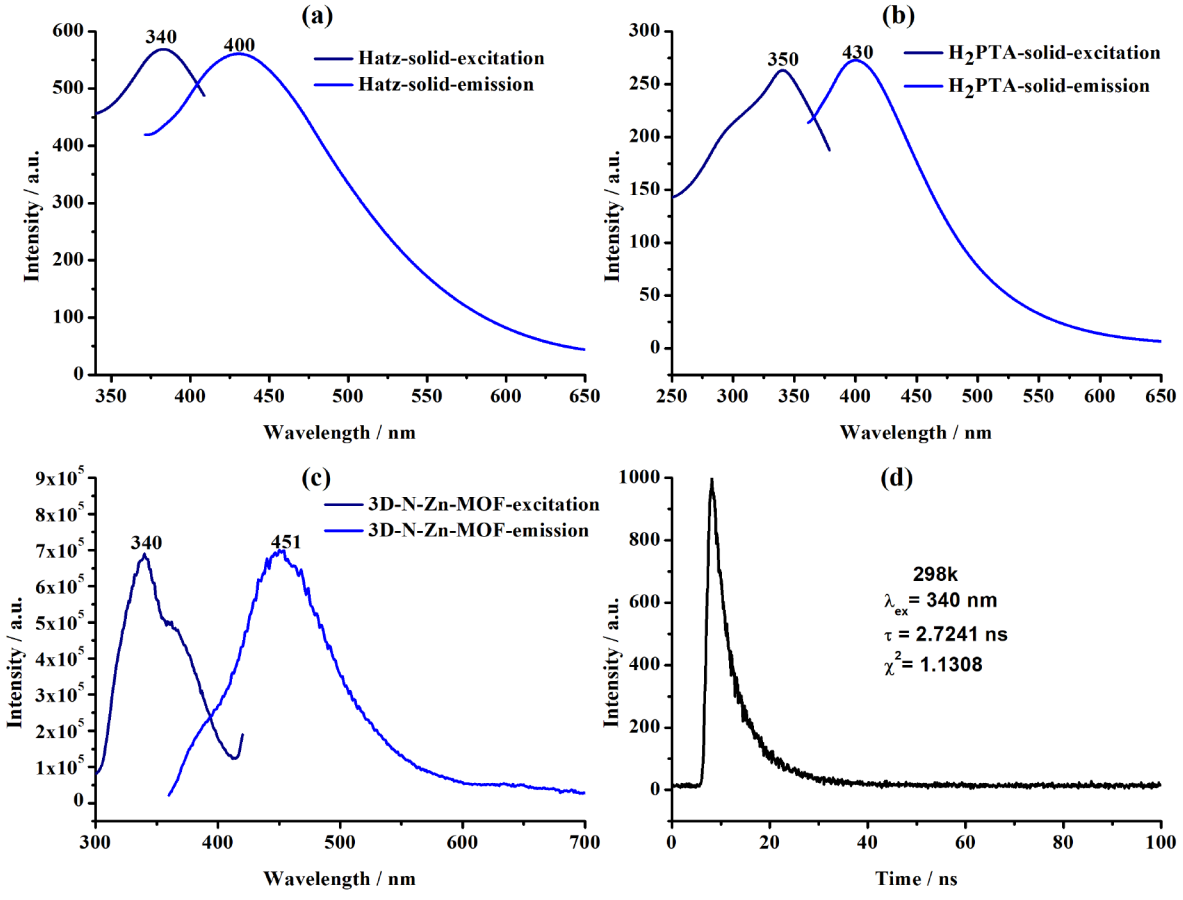

Figure 3. (a) The fluorescence of Hatz; (b) the fluorescence of H_2PTA; (c) the fluorescence of **3D-N-Zn-MOF**; (d) the fluorescence lifetime of **3D-N-Zn-MOF**.

https://doi.org/10.1021/acsomega.4c00431
ACS Omega 2024, 9, 18429−18437

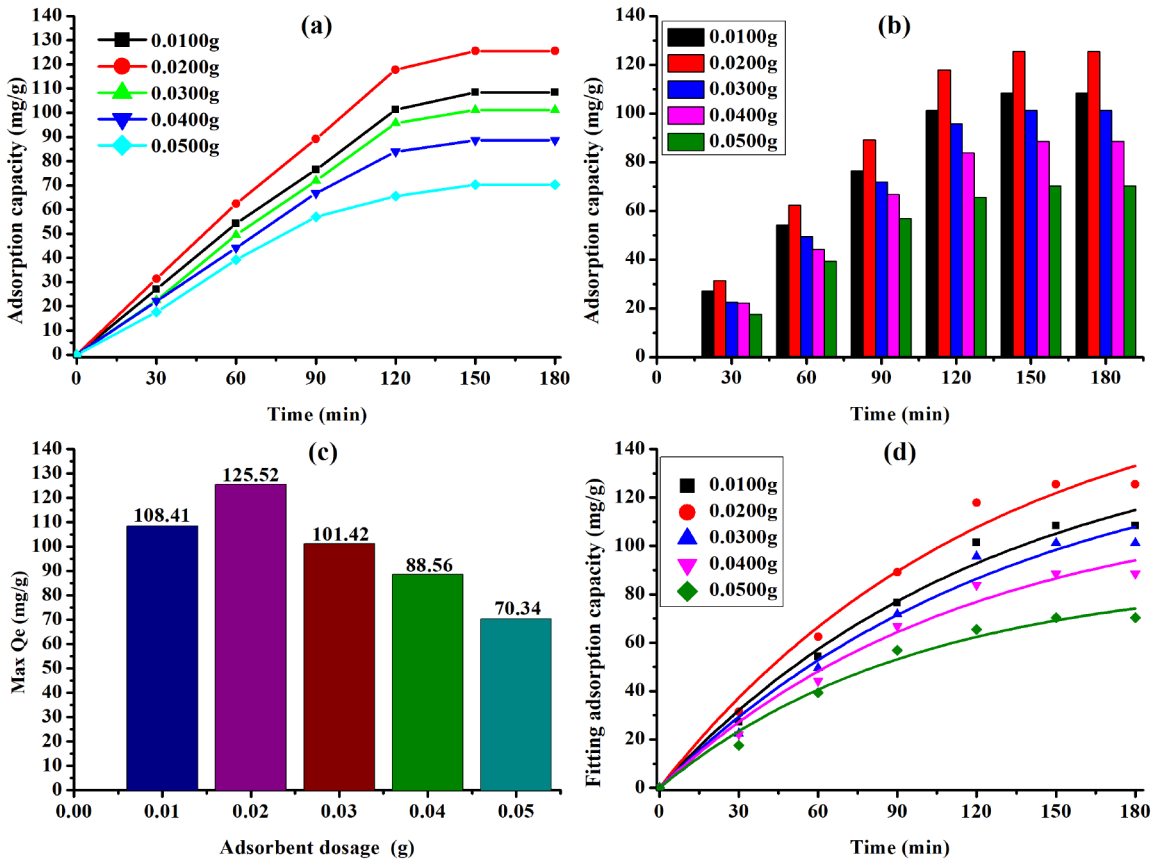

Figure 4. (a)−(c) Experimental adsorption curves under different dosages; (d) adsorption curve fitted by quasi first order adsorption kinetics.

Table 2. Cr(VI) Adsorption Performance of some Reported MOFs

entry	MOF	adsorbate	**adsorption capacity** (mg/g)	refs
1	ABT-$(ClO_4)_2$	Cr(VI)	271	30
2	ZJU	Cr(VI)	245	30
3	MONT-1	Cr(VI)	211.8	30
4	TMU-30	Cr(VI)	145	30
5	NiCo-LDH	Cr(VI)	99.9	30
6	UPC-50	Cr(VI)	56.8	30
7	UIO-66-NH_2	Cr(VI)	32.4	30
8	PAN/chitosan/UiO-66-NH_2	Cr(VI)	372.6	31
9	ACS Omega	Cr(VI)	145.0	32

reported Zn(II) complexes in literature.[29] This may be because it was a binuclear Zn(II) MOF, and each Zn(II) in **3D-N-Zn-MOF** coordinated with the N atoms in atz^- and the O atoms in PTA^{2-}. This led to the electron being transferred from atz^- and PTA^{2-} to Zn(II), reducing the electronegativity and rigidity of the ligand aromatic ring. Resulting in a longer fluorescence lifetime of **3D-N-Zn-MOF**.

3.3.2. Quantum Yield of 3D-N-Zn-MOF. At room temperature (298 K), the **3D-N-Zn-MOF** was excited at 340 nm, and its quantum yield was measured between 320 and 700 nm. The results (Figure S6) indicated that the quantum yield of **3D-N-Zn-MOF** was 3.02%, which was higher than the similar Zn(II) complexes reported in most literature.[19] This may be because the **3D-N-Zn-MOF** could provide a stable coordination architecture and suitable coordinate substrate for Zn(II), which could effectively reduce nonradiative energy transfer and loss, thereby improving quantum yield. Moreover, there was a small energy gap between the 4s and 3d orbital levels of Zn(II) in **3D-N-Zn-MOF**, making the charge transfer process easier. Zn(II) could promote electron transfer from ligands to central metal ions (LMCT), thereby improving the lifetime and yield of excited states.

3.4. Adsorption Performance of 3D-N-Zn-MOF. Herein, the performance of **3D-N-Zn-MOF** in adsorbing Cr(VI) was studied. The concentration of the inorganic pollutant Cr(VI) was 40 mg/L, with a dosage of 100 mL each time. The effects of **3D-N-Zn-MOF** dosage (0.0100 g−0.0500 g), different pH (5.00−8.00), and temperature (25−45 °C) on the adsorption of Cr(VI) were studied.

3.4.1. Effect of Dosage on Adsorption Performance. Accurately 0.0100 0.0200, 0.0300, 0.0400, and 0.0500 g of **3D-N-Zn-MOF** was weighed into 100 mL of Cr(VI) solution with a concentration of 40 mg/L at 25 °C, and pH = 7. The adsorption capacity (mg/g) of Cr(VI) adsorbed at different times was calculated by the adsorption capacity calculation formula $q = (C_0 - C_t) \cdot V/W$. The adsorption experiment

https://doi.org/10.1021/acsomega.4c00431
ACS Omega 2024, 9, 18429−18437

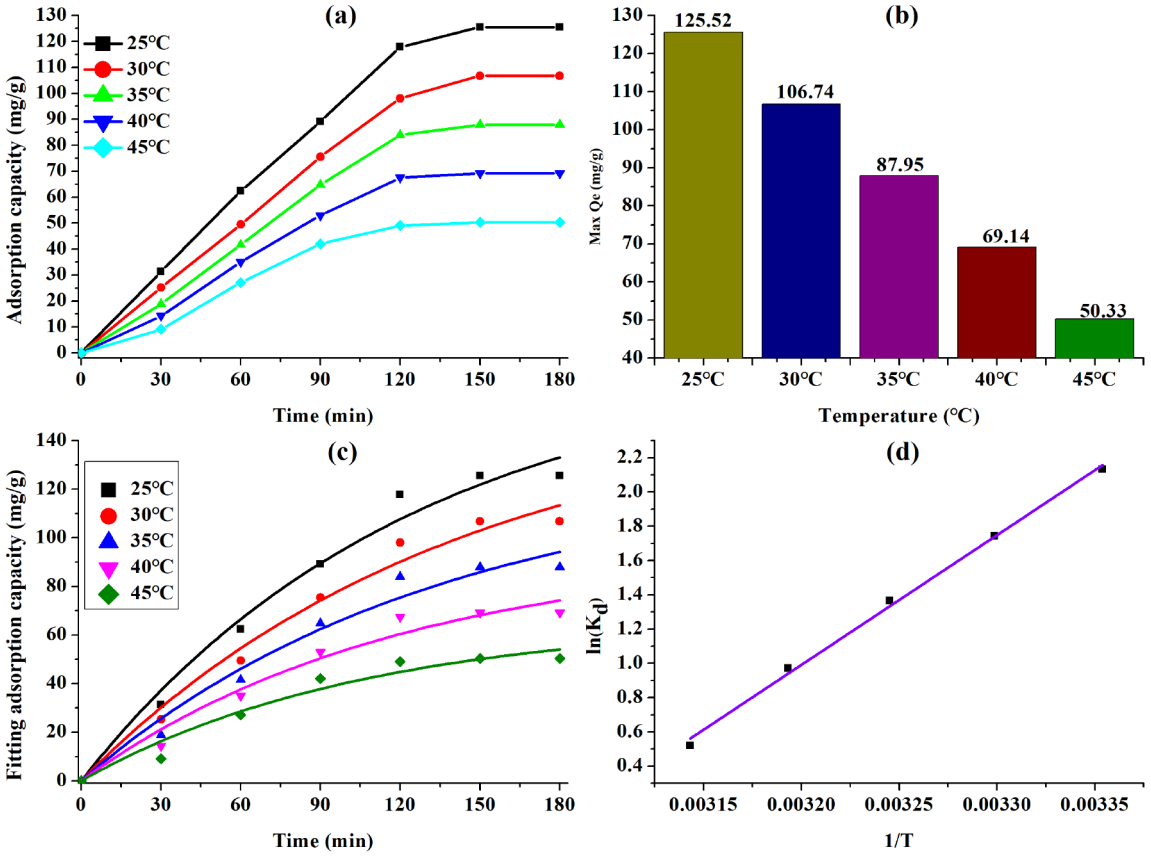

Figure 5. (a)−(c) Experimental adsorption curves under different temperatures; (d) adsorption curve fitted by quasi first order adsorption kinetics.

results (Figure 4) indicated that the adsorption capacity of **3D-N-Zn-MOF** for Cr(VI) increased continuously with time. The adsorption equilibrium was reached after adsorption for 150 min by **3D-N-Zn-MOF** (Figure 4a,b). At this time, the adsorption capacities of 0.0100−0.0500 g of **3D-N-Zn-MOF** (Figure 4c) were 108.41 125.52, 101.41, 88.56, and 70.34 mg/g, respectively. So, the adsorption capacity was the best when the concentration of adsorbent **3D-N-Zn-MOF** was 0.2000 g/L, which could reach 125.52 mg/g. By comparison of the performance of some MOFs adsorbents in adsorbing Cr(VI) (Table 2), it could be found that the **3D-N-Zn-MOF** had better performance in adsorbing Cr(VI) than the vast majority of MOFs adsorbents. The performance of **3D-N-Zn-MOF** in adsorbing Cr(VI) was analyzed by the quasi first order adsorption kinetics equation $q_t = q_e - q_e e^{-k1t}$. It was found that they have a good linear relationship ($R^2 > 0.97$) (Table S4). In addition, the quasi first order adsorption kinetics analysis also proved that the optimal concentration of the adsorbent was 0.2000 g/L, and the theoretical calculated maximum adsorption capacity at this time can reach 174.42 mg/g (Table S4), which was higher than the actual experimental adsorption capacity of 125.52 mg/g. This indicated that due to interference from experimental conditions such as solution purity and instrument precision, the experimental adsorption capacity was lower than the theoretical calculated adsorption capacity.

3.4.2. Effect of pH on Adsorption Performance. The above experimental results had shown that the optimal concentration of **3D-N-Zn-MOF** was 0.2000 g/L. So, in order to study the effect of pH on the adsorption performance of **3D-N-Zn-MOF** for Cr(VI),the pH of Cr(VI) solution was adjusted to 5, 6, and 8 by 0.100 mol/L HCl and NaOH at 25 °C. The experimental results (Figure S7a,b) indicated that the **3D-N-Zn-MOF** could reach adsorption equilibrium in solutions with pH 5, 6, and 8 after 150 min. At this point, their maximum equilibrium adsorption capacities (Figure S7c) were 91.77, 111.11, and 100.01 mg/g, respectively. They were all lower than the adsorption capacity at pH = 7. So, the optimal pH for **3D-N-Zn-MOF** to adsorb Cr(VI) was 7. It could been found that the **3D-N-Zn-MOF** had a wide pH adaptability for the adsorption of Cr(VI) by analyzing the performance at different pH. It was also found (Figure S7d) that they had a good linear relationship ($R^2 > 0.95$) (Table S5) by the quasi first-order adsorption kinetics equation to analyze the effect of pH on the adsorption of Cr(VI) by **3D-N-Zn-MOF**. The quasi first-order adsorption kinetics calculation analysis showed that the maximum equilibrium adsorption capacity could reach 232.29 mg/g at pH 5, which was only lower than the reported PAN/chitosan/UiO-66-NH_2 and ABT-$(ClO_4)_2$ adsorbents in literature.[31]

3.4.3. Effect of Temperature on Adsorption Performance. The above research results indicated that the optimal dosage concentration of **3D-N-Zn-MOF** was 0.2000 g/L, and the optimal pH was 7. Therefore, in a Cr(VI) solution with a pH of 7, the **3D-N-Zn-MOF** (0.0200 g) was added to study the effect of the temperature (25−45 °C) on adsorption. The experimental results (Figure 5a,b) indicated that **3D-N-Zn-MOF** could adsorb Cr(VI) for 150 min and reach adsorption equilibrium. However, as the temperature increased, the amount of Cr(VI) adsorbed by **3D-N-Zn-MOF** significantly decreased (Figure 5a,b). The maximum equilibrium adsorption capacities at 25−45 °C were 125.52 106.74, 87.95, 69.14, and

https://doi.org/10.1021/acsomega.4c00431
ACS Omega 2024, 9, 18429−18437

50.33 mg/g, respectively. A quasi first order kinetic analysis was conducted on the adsorption behavior at these temperatures, indicated a good linear relationship ($R^2 > 0.95$) (Table S6), and also demonstrated the maximum experimental and theoretical adsorption capacity at 25 °C. The adsorption thermodynamic data of **3D-N-Zn-MOF** for Cr(VI) adsorption process were fitted and analyzed by the Van't Hoff equation (Table S7). The analysis results indicated that the adsorption of Cr(VI) by **3D-N-Zn-MOF** at 25−45 °C was a spontaneous ($\triangle G < 0$) and exothermic ($\triangle H < 0$) process.

3.5. Adsorbent Regeneration and Cycling Experiments. The X-ray powder diffraction was used to characterize and analyze the collected solid adsorbent after the desorption and regeneration of the adsorbent. The test results showed that the diffraction peaks of the collected solid adsorbent (Figure S8) were consistent with the theoretical simulation of **3D-N-Zn-MOF**. This clearly demonstrates that the **3D-N-Zn-MOF** could be repeatedly regenerated, and it was a very pure material. In addition, XPS (Figure S9) also indicated that the **3D-N-Zn-MOF** after adsorption regeneration was composed of elements such as Zn, C, N, and O. As a result, the 3D-N-Zn-MOF had the characteristics of regeneration and reuse.

The cyclic experimental results (Figures 6 and S10) indicated that the efficiency of **3D-N-Zn-MOF** could reach

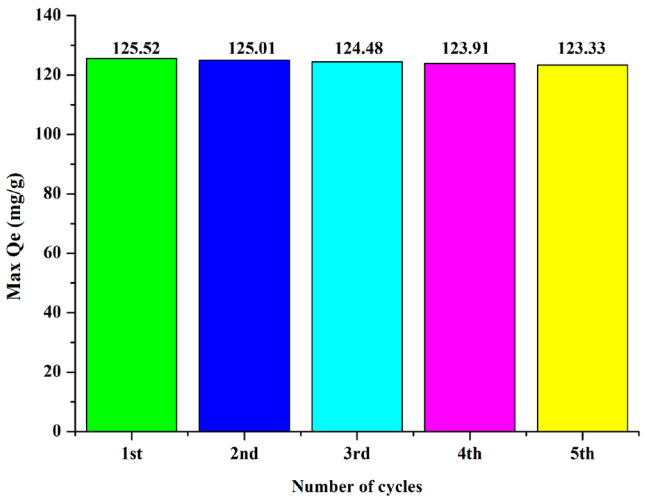

Figure 6. Maximum equilibrium adsorption capacity of the cycle experiment.

100% after one cycle. Even though its efficiency had decreased after five cycles, it still maintains 98.26%. It could be seen that the **3D-N-Zn-MOF** had efficient adsorption performance for Cr(VI).

4. CONCLUSION

In summary, a three-dimensional Zn(II) metal organic framework $\{[Zn_2\cdot(atz)_2\cdot(pta)]\cdot 3H_2O\}_n$ (**3D-Zn-MOF**) with strong luminescence and Cr(VI) adsorption properties was synthesized and fully characterized. In addition, its nanomaterials (**3D-N-Zn-MOF**) with particles of approximately 100 nm were prepared by a cell fragmentation apparatus. The fluorescence lifetime and quantum yield of **3D-N-Zn-MOF** were 2.7241 ns and 3.02%, respectively. The maximum experimental adsorption capacity of **3D-N-Zn-MOF** for Cr(VI) could reach 125.52 mg/g, which was superior to the majority of MOF adsorbents. Furthermore, at 25 °C−45 °C, the adsorption of Cr(VI) by **3D-N-Zn-MOF** was a spontaneous ($\triangle G < 0$) and exothermic ($\triangle G < 0$) process. This study provides an example for studying bifunctional materials with fluorescence and Cr(VI) adsorption properties.

■ ASSOCIATED CONTENT

Supporting Information

The Supporting Information is available free of charge at https://pubs.acs.org/doi/10.1021/acsomega.4c00431.

Chemicals and instruments, adsorption experiment, adsorbent regeneration experiment, IR of **3D-Zn-MOF**, TGA of **3D-N-Zn-MOF**, the geometric configuration of Zn(II), and the atz^- take μ_3-η^1:η^1:η^1 to coordinates with three Zn(II) ions, SEM of **3D-N-Zn-MOF**, the N_2 adsorption/desorption isotherms of **3D-N-Zn-MOF**, quantum yield of **3D-N-Zn-MOF**, experimental adsorption curves under different pH, XRD of **3D-N-Zn-MOF**, XPS of **3D-N-Zn-MOF** after adsorption and regeneration, circular experiment (Figure S1−S8), crystal parameters of **3D-N-Zn-MOF**, partial bond length (Å) and bond angle (deg) of **3D-N-Zn-MOF**, hydrogen bond of **3D-Zn-MOF**, quasi first order kinetic equation under the influence of dosage, pH, and temperature, and adsorption thermodynamic parameters of adsorbents at different temperatures (Tables S1−S7) (PDF)

data_lsx-1 (CIF)

■ AUTHOR INFORMATION

Corresponding Authors

Shixiong Li − *School of Mechanical and Resource Engineering, Wuzhou University, Wuzhou 543003, PR China; Wuzhou Resource Recycling Engineering Technology Research Center, Wuzhou 543003, PR China;* orcid.org/0000-0002-6600-1749; Email: lsx1324@163.com

Shihua Xu − *School of Mechanical and Resource Engineering, Wuzhou University, Wuzhou 543003, PR China; Wuzhou Resource Recycling Engineering Technology Research Center, Wuzhou 543003, PR China*; Email: 948891875@qq.com

Yuejing Bin − *School of Mechanical and Resource Engineering, Wuzhou University, Wuzhou 543003, PR China; Wuzhou Resource Recycling Engineering Technology Research Center, Wuzhou 543003, PR China; Guangxi Colleges and Universities Key Laboratory of Gemstone Design and Testing, Wuzhou 543003, PR China*; Email: binyj@126.com

Authors

Yufeng Chen − *School of Mechanical and Resource Engineering, Wuzhou University, Wuzhou 543003, PR China; Wuzhou Resource Recycling Engineering Technology Research Center, Wuzhou 543003, PR China*

Yubing Liu − *School of Mechanical and Resource Engineering, Wuzhou University, Wuzhou 543003, PR China*

Ping Shi − *School of Mechanical and Resource Engineering, Wuzhou University, Wuzhou 543003, PR China*

Complete contact information is available at: https://pubs.acs.org/10.1021/acsomega.4c00431

Author Contributions

Y.C. contributed to writing−original draft. S.L. contributed to funding acquisition and writing−review and editing. Y.L. contributed to data curation. P.S. contributed to data curation.

https://doi.org/10.1021/acsomega.4c00431
ACS Omega 2024, 9, 18429−18437

S.X. contributed to funding acquisition. Y.B. contributed to funding acquisition and writing−review and editing.

Notes

The authors declare no competing financial interest.

■ ACKNOWLEDGMENTS

This work was supported by the Guangxi University Young and Middle-aged Teachers' Basic Scientific Research Ability Improvement Project (no. 2020KY17021), Guangxi Natural Science Foundation, China (no. 2023JJA120079), Science and Technology Project of WuZhou (202302049), Central Government Funds for Guiding Local Scientific and Technological Development (2021ZYZX2089), School level scientific research project of Wuzhou University (no. 2021B002), and National College Student Entrepreneurship Training Program (no. 202111354318).

■ REFERENCES

(1) Dhakshinamoorthy, A.; Asiri, A. M.; Garcia, H. 2D metal−organic frameworks as multifunctional materials in heterogeneous catalysis and electro/photocatalysis. *Adv. Mater.* **2019**, *31* (41), 1900617.

(2) Hong, F.; Ren, L.; Chen, Y. Kill three birds with one stone: Zr-MOF-mediated composite multi-functional materials to enhance the efficiency for fluorescent and colorimetric dual-signal readout bioassay. *Chem. Eng. J.* **2023**, *452*, 139149.

(3) Li, H. Y.; Hua, X.; Fu, T.; Liu, X. F.; Zang, S. Q. Photochromic and electrochromic properties of a viologen-based multifunctional Cd-MOF. *Chem. Commun.* **2022**, *58* (56), 7753−7756.

(4) Yaghi, O. M.; Li, H. Hydrothermal synthesis of a metal-organic framework containing large rectangular channels. *J. Am. Chem. Soc.* **1995**, *117* (41), 10401−10402.

(5) Li, S.; Sun, S.; Wu, H.; Wei, C.; Hu, Y. Effects of electron-donating groups on the photocatalytic reaction of MOFs. *Catal. Sci.Technol.* **2018**, *8* (6), 1696−1703.

(6) Li, S.; Luo, P.; Wu, H.; Wei, C.; Hu, Y.; Qiu, G. Strategies for improving the performance and application of MOFs photocatalysts. *ChemCatchem* **2019**, *11* (13), 2978−2993.

(7) Shi, X.; Cao, B.; Liu, J.; Zhang, J.; Du, Y. Rare-Earth-Based Metal−Organic Frameworks as Multifunctional Platforms for Catalytic Conversion. *Small* **2021**, *17* (22), 2005371.

(8) Sarawade, P.; Tan, H.; Anjum, D.; Cha, D.; Polshettiwar, V. Size- and shape-controlled synthesis of hexagonal bipyramidal crystals and hollow self-assembled al-mof spheres. *ChemSuschem* **2014**, *7* (2), 529−535.

(9) Farahani, Y. D.; Safarifard, V. Highly selective detection of Fe^{3+}, Cd^{2+} and CH_2Cl_2 based on a fluorescent Zn-MOF with azine-decorated pores. *J. Solid State Chem.* **2019**, *275*, 131−140.

(10) Li, S.; Huang, L.; Jia, B.; Feng, X.; Cao, Y.; Chen, Y.; Bin, Y. Effect and mechanism of inorganic anions on the adsorption of Cd^{2+} on two-dimensional copper-based metal−organic framework. *Inorg. Chem. Commun.* **2024**, *159*, 111819.

(11) Pal, S. C.; Ahmed, R.; Manna, A. K.; Das, M. C. Potential of a pH-Stable Microporous MOF for C_2H_2/C_2H_4 and C_2H_2/CO_2 Gas Separations under Ambient Conditions. *Inorg. Chem.* **2022**, *61* (45), 18293−18302.

(12) Zhang, Y. Z.; Kong, X. J.; Zhou, W. F.; Li, C. H.; Hu, H.; Hou, H.; Liu, H. Z.; Geng, L.; Huang, H.; Zhang, X.; et al.et al. Pore Environment Optimization of Microporous Metal−Organic Frameworks with Huddled Pyrazine Pillars for C_2H_2/CO_2 Separation. *ACS Appl. Mater. Inter.* **2023**, *15* (3), 4208−4242.

(13) Liao, B.; Li, S. Multifunctional Mn(II) Metal-Organic framework for photocatalytic aerobic oxidation and C-H direct trifluoromethylation. *J. Catal.* **2022**, *414*, 294−301.

(14) Yang, S.; Chen, Y.; Li, S.; Chen, H. Efficient photocatalytic performance and the mechanism of copper (i) metal−organic framework nanosheets. *New J. Chem.* **2023**, *47* (32), 15348−15356.

(15) Li, S.; Yang, S.; Liang, G.; Yan, M.; Wei, C.; Lu, Y. UiO-66 type metal organic framework. *RSC Adv.* **2023**, *13* (8), 5273−5282.

(16) Wang, M.; Han, K.; Zhang, S.; Sun, L. Integration of organometallic complexes with semiconductors and other nanomaterials for photocatalytic H2 production. *Coord. Chem. Rev.* **2015**, *287*, 1−14.

(17) Bai, J.; Wang, J.; Zheng, H.; Zhao, X.; Wu, P.; Pei, L.; Wang, J. Modulating Photoinduced Electron Transfer between Photosensitive MOF and Co (II) Proton Reduction Sites for Boosting Photocatalytic Hydrogen Production. *Small* **2023**, *19* (48), 2305024.

(18) Pang, W.; Shao, B.; Chen, X.; Gu, Q. X.; Yang, F. J.; Li, S.; Huang, J. Enhancing the activity of metal-organic nanosheets for oxygen evolution reaction by substituent effects. *J. Colloid Interface sci.* **2022**, *608*, 306−312.

(19) Li, S.; Chen, Y.; S, M. Y.; Wei, C. Synthesis, structure and fluorescence analysis of three Zn(II) complexes based on (1-methyl-1H-benzimidazol-2-yl) methanol. *Chin. J. Inorg. Chem.* **2023**, *39* (9), 1782−1790.

(20) Li, S. X.; Feng, A. Q.; Y, H.; Liang, G. C.; Lu, L. F.; Lu, H. P. Two-Dimensional Copper-Based Coordination Polymer: Synthesis, Structure and Ion Effect on Adsorption of Cr(VI). *Chin. J. Inorg. Chem.* **2022**, *38*, 941−950.

(21) Li, B.; Chen, X.; Hu, P.; Kirchon, A.; Zhao, Y. M.; Pang, J.; Zhang, T.; Zhou, H. C. Facile fabrication of a multifunctional metal−organic framework-based sensor exhibiting exclusive solvochromic behaviors toward ketone molecules. *ACS Appl. Mater. Inter* **2019**, *11* (8), 8227−8233.

(22) Jo, Y. M.; Jo, Y. K.; Lee, J. H.; Jang, H. W.; Hwang, I. S.; Yoo, D. J. MOF-based chemiresistive gas sensors: toward new functionalities. *Adv. Mater.* **2023**, *35* (43), 2206842.

(23) Han, J. H.; Hu, B. Q.; Li, T.; Liang, H.; Yu, F.; Zhao, Q.; Li, B. Synthesis, Structures, and Sorption Properties of Two New Metal−Organic Frameworks Constructed by the Polycarboxylate Ligand Derived from Cyclotriphosphazene. *ACS Omega* **2021**, *6* (36), 23110−23116.

(24) Dolomanov, O. V.; Bourhis, L. J.; Gildea, R. J.; Howard, J. A.; Puschmann, H. OLEX2: a complete structure solution, refinement and analysis program. *J. Appl. Crystallogr.* **2009**, *42* (2), 339−341.

(25) Gao, J. Y.; Wang, N.; Xiong, X. H.; Chen, C. J.; Xie, W. P.; Ran, X. R.; Long, Y.; Yue, S. T.; Liu, Y. L. Syntheses, structures, and photoluminescent properties of a series of zinc(ii)−3-amino-1,2,4-triazolate coordination polymers constructed by varying carboxylate anions. *CrystEngcomm* **2013**, *15*, 3261.

(26) Luo, M. B.; Yuan, Z. Z.; Xu, W. Y.; Luo, F.; Li, J. Q.; Zhu, Y.; Feng, X. F.; Liu, S. J. Framework isomers controlled by the speed of crystallization: different aggregation fashions of Zn (II) and 1, 2, 4-triazol-3-amine, distinct (3, 4)-connected self-penetrating nets, and various pore shapes. *Dalton Tran.* **2013**, *42* (38), 13802−13805.

(27) Liu, J.; Wei, Y.; Bao, F.; Li, G.; Liu, H.; Wang, H. Pore-size tuning in pillared-layer metal−organic framework with self-penetrated rob net for selective gas adsorption and efficient dyes adsorption in aqueous solution. *Polyhedron* **2019**, *169*, 58−65.

(28) Yang, Y.; Huang, J.; Zou, Y.; Li, Y.; Zhan, T.; Huang, L.; Ma, X.; Zhang, Z. N, O-coordinated Zn-MOFs for selective conversion of CO_2 to formate. *Appl. Sur. Sci.* **2023**, *618*, 156664.

(29) Li, S.; Liu, L.; Deng, Y.; Huang, Y.; Chen, Y.; Liao, B. Terminal anion induced zinc (II) mononuclear complexes trans-to-cis isomerization regulate photoluminescence properties and its solution behavior. *Polyhedron* **2019**, *174*, 114158.

(30) Li, R.; Zhong, W.; Xie, L.; Xie, Y.; Li, J. Recent Advances in Adsorptive Removal of Cr(VI) Ions by Metal-Organic Frameworks. *Chin. J. Inorg. Chem.* **2021**, *37*, 385−400.

(31) Jamshidifard, S.; Koushkbaghi, S.; Hosseini, S.; Rezaei, S.; Karamipour, A.; Rad, J. A.; Irani, M. Incorporation of UiO-66-NH_2 MOF into the PAN/chitosan Nanofibers for Adsorption and Membrane Filtration of Pb(II), Cd(II) and Cr(VI) Ions from Aqueous Solutions. *J. Hazard. Mater.* **2019**, *368*, 10−20.

(32) Zeng, Y.; Li, X.; Chen, Y.; Li, S. High-Efficiency Adsorption of Cr(VI) and Mn(VII) from Wastewater by a Two-Dimensional

https://doi.org/10.1021/acsomega.4c00431
ACS Omega 2024, 9, 18429−18437

Copper-Based Metal−Organic Framework. *ACS Omega* **2023**, *8* (40), 36978−36985.

https://doi.org/10.1021/acsomega.4c00431
ACS Omega 2024, 9, 18429−18437